Biophysical Chemistry 15 (1982) 327–341
Elsevier Biomedical Press

SINGLE CHANNEL GATING EVENTS IN TRACER FLUX EXPERIMENTS

III. ACETYLCHOLINE RECEPTOR-CONTROLLED Li^+ EFFLUX FROM SEALED *TORPEDO MARMORATA* MEMBRANE FRAGMENTS

Julius BERNHARDT and Eberhard NEUMANN

Max-Planck-Institut für Biochemie, 8033 Martinsried bei München, F.R.G.

Received 7th January 1982
Revised manuscript received 16th March 1982

Key words: Gating process; Ion transport; Tracer flux; (Torpedo marmorata)

Filter assay measurements of Li^+ efflux from acetylcholine receptor-containing vesicular *Torpedo marmorata* membrane fragments (microsacs) are presented. Techniques are introduced for: (a) inducing a complete emptying of the Li^+ content of all microsacs containing one or more functionally intact receptors, and (b) for determining the distribution of internal volumes of the microsacs using filtration with membrane filters of different pore sizes. The flux amplitudes resulting for acetylcholine receptor-controlled Li^+ efflux, when receptors are inhibited by α-bungarotoxin or inactivated by a neuroactivator-induced desensitization process, were measured. Amplitude analysis was used to determine characteristic parameters of the microsacs that may vary with the technique of preparation (e.g., the distribution in size and receptor content), as well as the mean single channel flux amplitude contribution $\langle e^{-kt} \rangle_\infty$, which represents the mean reduction of the Li^+ content of a microsac due to efflux from a single receptor-controlled channel prior to channel closing due to inhibition or inactivation of the receptor. The ratio k_{eff}/k_i was found to lie in the range $0.1 < k_{eff}/k_i < 0.5$, where k_{eff} and k_i are, respectively, the rate constant for Li^+-Na^+ exchange flux and for the slow inactivation reaction mode of the acetylcholine receptor induced by carbamoylcholine at high concentrations.

1. Introduction

Sealed membrane fragments (microsacs) prepared from *Torpedo* electric organs have been widely used to study the functional properties of the membrane-bound acetylcholine receptor (AcChR). The direct measurement of ion flux from or into microsacs is rapidly becoming a powerful tool for investigating the physiologically relevant role of the receptor as a gating molecule to transmembrane ion transport. Due to practical constraints, early methods for measuring tracer ion flux, based on a filter assay procedure [1], were limited to a time range greater than 10 s. Under these conditions, the time course of the receptor-controlled flux contribution was not resolvable when *Torpedo* microsacs preincubated with $^{22}Na^+$ were diluted into a bath containing neuroactivator [2]. However, it was found that the flux amplitudes, reflecting the total tracer content of the microsacs entrapped on the filter, were dependent on neuroactivator concentration. This result was attributed to an incomplete equilibration of the tracer in the microsacs with the bath, due to a slow receptor inactivation process (desensitization), following an initial rapid activation phase. A recent investigation, using a rapid quench flow technique capable of measuring flux in the 50 ms time range, has essentially confirmed this interpretation [3]. It was found that at least two inactivation processes occur, of which the slower one, on the time scale of seconds, leads to a complete cessation of flux. (The presence of several inactivation phases could, of course, not be inferred from the amplitude data alone.)

The finding that receptor inactivation leading

0301-4622/82/0000–0000/$02.75

to channel closing is reflected in the flux amplitudes led to the proposal of a mathematical scheme for analysing flux data [2]. The original scheme was later modified and generalized to cover all tracer flux processes from or into closed membrane structures (CMS), which are controlled by a channel gating process of arbitrary complexity [4–7]. The basic postulates underlying the treatment are: (a) The tracer content of a collection of microsacs is the sum of the tracer content of the individual microsacs. (b) Under suitable experimental conditions, flux of tracer through a single open channel on a microsac changes the tracer content by an exponential factor $e^{-k\tau}$, where k is the rate constant for flux through a single channel, and $\tau(t)$ is the total time interval the channel was open up to the time of measurement t. (c) If flux occurs through several channels on a microsac, the overall change in tracer content of the microsac is the product of the exponential factors for the individual channels. (d) For a collection of microsacs, each having n receptor-controlled channels, the average change in the tracer content of a microsac is $\langle e^{-kt}\rangle^n$, i.e., the mean single channel flux contribution $\langle e^{-kt}\rangle$ to the nth power. $\langle e^{-kt}\rangle$ is the average of $e^{-k\tau}$ over all possible open times. Simple expressions for $\langle e^{-kt}\rangle$ can be derived, which explicitly depend on the kinetic constants of the receptor reaction that controls channel opening and closing. The prime aim of the flux analysis must therefore be to determine $\langle e^{-kt}\rangle$. (f) The flux rate constant k, for a channel on a microsac with volume v, is inversely proportional to v. Therefore, $\langle e^{-kt}\rangle$ implicitly depends on v. (g) The change in the overall tracer content of an inhomogeneous mixture of microsacs is the sum of component contributions $P_n[\langle e^{-kt}\rangle^n]_v$, where P_n is the fraction of the total internal volume of all microsacs contributed by the microsacs with n receptors per microsac, and the square brackets denote the volume average of the expression $\langle e^{-kt}\rangle^n$. In principle, the volume average is the result of averaging over a distribution function, that represents the probability that a microsac with n receptors has a given volume v.

These considerations imply that the overall change in the tracer content of a collection of microsacs depends on two sets of parameters: (1) the term $\langle e^{-kt}\rangle$, which expresses the intrinsic functional properties of the average receptor-controlled channel, and which does not depend on factors that may vary from preparation to preparation, and (2) the fractions P_n, and the distribution in microsac volumes, which account for all dependences on the materials and methods of preparation. Qualitatively, inhomogeneities in the receptor content of the microsacs will lead to multiple phases in the time course of overall flux. Each distinct subfraction of microsacs, with n receptors per microsac, will contribute a separate phase with time course $[\langle e^{-kt}\rangle^n]_v$. The terms P_n constitute the respective maximum relative amplitudes of these phases. On the other hand, the receptor reaction controlling channel opening and closing may also occur in several phases, leading to a multiphasic time course of $\langle e^{-kt}\rangle$, and of the overall flux process. Any attempt to associate separate phases of the measured flux process with the gating reaction alone, on an ad hoc basis, is of questionable validity. It is essential to account first for the terms arising from inhomogeneities in microsac receptor content and volume, before a reliable quantitative analysis of the contributions due to channel gating can be made.

In this article methods for determining the factors P_n, and the distribution in microsac volumes, on the basis of flux amplitude measurements using the filter assay technique, are presented. In section 3.1, the dependence of the flux amplitudes for Li^+ efflux from *Torpedo marmorata* microsacs induced by carbamoylcholine (CbCh) on [CbCh] is investigated. In section 3.2, a technique for promoting the complete emptying of the Li^+ content of microsacs is presented. In section 3.3, reduction in flux amplitudes following the progressive inhibition of receptors with increasing amounts of α-bungarotoxin (α-BuTx) is examined, and the results are analysed in sections 4.2 and 4.5. In section 3.4, filtration measurements using filters with different pore sizes are presented. The results are analysed to determine the volume distribution function of the microsac suspension $Q(v)$ in section 4.3. In section 4.4, it is shown that knowledge of the P_n and of $Q(v)$ permits evaluation of several fundamental parameters characterizing the suspension [7]: the mean volume $\bar{v}$ of a microsac, the

mean number $\bar{n}$ of receptors per microsac, the mean surface density of receptors $\bar{\rho}$, and the probability ξ_n that a given microsac has n receptors.

In order to illustrate the general procedure for determining $\langle e^{-k't} \rangle$ for an arbitrary gating process, once the P_n and $Q(v)$ are known, the mean single channel flux amplitude contribution $\langle e^{-k't} \rangle_\infty$ is determined from the reduction in flux amplitudes following inhibition with α-BuTx, for flux induced by a saturating concentration of CbCh. Analysis of the flux data using equations derived in the preceding article [7] then permits estimation of the ratio (k'_{eff}/k_i), where k'_{eff} is the effective, volume-independent flux rate constant, and k_i is the effective forward rate constant for CbCh-induced receptor inactivation.

2. Experimental procedures

2.1. Materials

Sealed AcChR-containing membrane fragments (microsacs) were prepared from liquid N_2-frozen electric organs of *Torpedo marmorata* (live from the Station Biologique d'Archachon, France) according to a recently developed procedure [8]. After incubation of a crude tissue homogenate in 0.2 M CsCl (Merck, Darmstadt), microsacs which are sealed and contain functionally intact AcChR are selectively filled with 0.2 M LiCl by successive additions of 10 mM acetylcholine (AcCh, Sigma). The intact microsacs are then separated from the nonfunctional ones by centrifugal sedimentation in Percoll (Pharmacia) suspension gradients.

Sartorius membrane filters type SM11306, SM11305, SM11304 and SM11303, with pore sizes 0.45, 0.65, 0.8 and 1.2 μm, respectively, were used in the determination of the microsac volume distribution. Millipore HAWP0025 membrane filters with pore size 0.45 μm were used for all other filtrations. Flux medium consisting of 0.2 M NaCl, 5 mM KCl, 1 mM $CaCl_2$ and 5 mM sodium phosphate, pH 7.0, was used as wash medium, and for the preparation of the solutions.

2.2. Methods

The flux measurements were carried out using a Sartorius multiple suction apparatus, modified so that application of suction is controlled by electrically triggered magnetic valves coupled to digital clocks. In all filtrations the flow rate of liquid through the filters was adjusted to 1.7 ml/s.

Routinely, microsacs filled with LiCl were added to an ice-cooled dilution bath under stirring. 5-ml aliquots of the diluted suspension were then filtered, and the filters washed with 5-ml portions of ice-cold wash medium. The successive washings were made immediately after the last torus of liquid had disappeared from the filter.

The Li^+ content of each dried filter, added to 5 ml of a 1% Triton X-100 solution in a counting vial, was measured at 670 nm by flame emission spectroscopy (FES) (Unicam SP 1900), after shaking the vials for 12 h. The Li^+ concentration of the dilution bath was also measured to correct for pipetting errors.

All measurements were performed using aliquots of a single microsac suspension.

3. Results

3.1. CbCh concentration dependence of flux amplitudes

The flux amplitude corresponding to the residual Li^+ content of a collection of microsacs after a transient efflux phase induced by CbCh activation of AcChR was determined as follows. A set of runs were carried out, where for each run 0.35 ml of microsac suspension was injected into 35 ml of a dilution bath containing a solution of CbCh in flux medium. Six 5-ml aliquots of the diluted suspension were then filtered, and washed four times with 5 ml of flux medium.

Fig. 1 presents the Li^+ content for three sample runs as a function of the time after initial dilution. On the time scale of the measurement (> 10 s) the time dependence of the change in Li^+ content cannot be resolved. With increasing CbCh concentration the Li^+ content decreases, and eventually reaches a limiting value. As seen in fig. 2, the

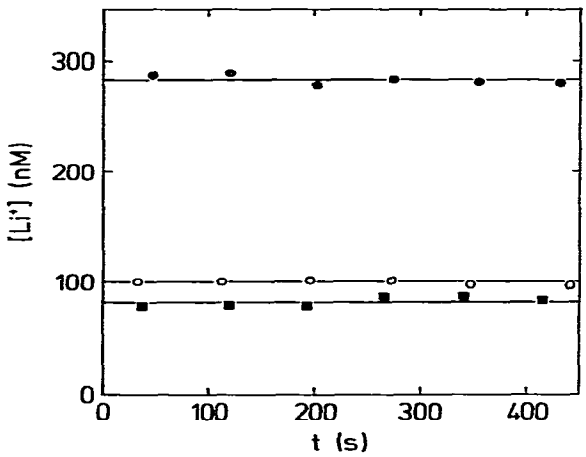

Fig. 1. Li^+ content of filters expressed as $[Li^+]$ measured by FES after dissolving microsacs entrapped on filters in 5 ml of 1% Triton X-100. Successive filtrations were made at times t after initial injection of microsacs into a dilution bath. The filters were washed four times with 5 ml of wash medium. The data represent three separate runs with (a) flux medium as bath and wash medium (●———●), (b) 0.5 mM CbCh as bath and flux medium as wash medium (○———○), (c) flux medium as bath and four washings using successively 0.1 mM AcCh, flux medium, 0.1 mM AcCh, and flux medium (■———■).

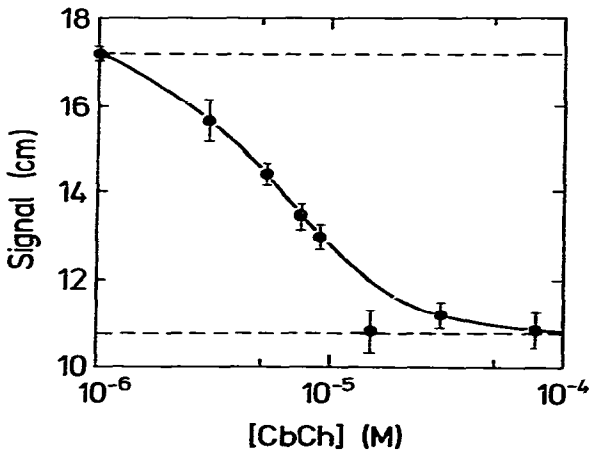

Fig. 2. Dose-response curve based on the flux amplitudes expressed as the measured FES signal, resulting when microsacs are diluted into a bath containing CbCh solution at the indicated concentrations. The upper and lower dashed lines, respectively, represent the limiting flux amplitudes at high and low CbCh concentrations.

half-response constant of Li^+ content vs. log[CbCh] is 5.7×10^{-6} M. A similar result has been obtained by Miller et al. [9] for ^{22}Na efflux from *Torpedo californica* membrane fragments.

3.2. Complete emptying of microsacs

The limiting Li^+ content approached at high [CbCh] need not correspond to a complete equilibration of microsac interior and bath. In order to determine the end amplitude resulting for complete emptying, a modification of the flux technique described above was devised. A set of six runs was carried out, where the number of washings per run and the composition of the wash medium were varied. In each of the runs, 0.4 ml of microsac suspension was initially injected into a dilution bath containing 35 ml of flux medium. Six filtrations with 5 ml of diluted suspension were then carried out using the same wash procedure. The sequence of wash steps used for the individual runs was: (1) 4×5 ml of flux medium; (2) 5 ml AcCh solutions (0.1 mM) in flux medium, followed by 3×5 ml flux medium; (3) 5 ml AcCh (0.1 mM), 5 ml flux medium, 5 ml AcCh (0.1 mM), 5 ml flux medium; (4) 8×5 ml flux medium; (5) 5 ml AcCh (0.1 mM), followed by 7×5 ml flux medium; (6) 5 ml AcCh (0.1 mM), 3×5 ml flux medium, 5 ml AcCh (0.1 mM), 3×5 ml flux medium. For comparison, two runs in which 0.4 ml of microsac suspension was initially injected into 35 ml AcCh (0.1 mM) were also carried out. The Li^+ content of the filters determined for these runs is presented in table 1. The first set of four runs comprises four washings per filtration, the second set eight washings per filtration. For both sets injection into a bath containing AcCh leads to less of a reduction in Li^+ content than injection into flux medium followed by washing with AcCh. A second washing with AcCh leads only to a small further reduction in Li^+ content, independent of whether one or three washings with flux medium are made between the AcCh washings. The residual Li^+ content present after successive AcCh washings apparently cannot be removed by flux through receptor-controlled channels. These findings indicate that wash sequence 3 in table 1 can

Table 1

No.	Bath [a]	Wash sequence [b]	Li^+ [c]	% Reduction [d]
1	B	B, B, B, B	100	–
2	B	A, B, B, B	32	68
3	B	A, B, A, B	28	4
4	B	B, B, B, B, B, B, B, B	100	–
5	B	A, B, B, B, B, B, B, B	40	61
6	B	A, B, B, B, A, B, B, B	36	3
7	A	B, B, B, B	70	–
8	A	B, B, B, B, B, B, B, B	68	–

[a] Content of initial dilution bath: A=0.1 mM AcCh; B=flux medium.

[b] Sequence of successive 5-ml wash aliquots.

[c] % Li^+ content of a run in a given set of four or eight washings, relative to the blank runs 1 and 4, respectively.

[d] % reduction in Li^+ content from one run in a given set to the next, given by (change in Li^+ content/maximum change in Li^+ content)×100.

be used to promote complete emptying of microsacs containing functional AcChR.

3.3. Reduction in flux amplitude upon toxin inhibition

Binding of α-BuTx (Miami Serpentarium) to AcChR leads to practically irreversible inhibition of flux through receptor-controlled channels. When microsacs are incubated with increasing amounts of α-BuTx, there is a progressive decrease in the maximum flux amplitude connected with CbCh-induced efflux [10,11]. Ultimately, when the amount of toxin added equals the total amount of toxin sites on the AcChR, flux is abolished completely. For the measurement of toxin inhibition, 0.9 ml of microsac suspension was injected into 10 ml of an ice-cooled flux medium bath containing α-BuTx. After an incubation period of longer than 4 h a 4.5 ml aliquot of the diluted suspension was added to 30 ml of dilution bath. In a first set of runs, this bath consisted of flux medium. For each run six 5-ml aliquots were filtered, and washed using wash sequence 3 in table 1, leading to complete emptying of all microsacs containing functional receptors not inhibited by toxin. In a second set of runs the dilution bath consisted of a 0.5 mM solution of CbCh in flux medium. For each run six 5-ml aliquots were filtered, and washed with 4×5 ml of flux medium (wash sequence 1). Fig. 3 shows the resulting reduction of the Li^+ content of the filters (flux amplitude) with increasing degree of inhibition. At a given toxin concentration, the Li^+ content for efflux induced by 0.5 mM CbCh exceeds or equals the content measured under conditions leading to complete emptying of microsacs. The initial concentration of Li^+ in the microsacs is 0.2 M. $[Li^+] \lesssim 1$ μM in the dilution bath upon completion of flux. Full equilibration of microsac internal Li^+ with the bath should thus lead to a reduction of Li^+ content by a factor of the order of 10^{-5}. Within the errors of measurements, this would correspond to a complete emptying. The results summarized in fig. 3 therefore imply that, even at saturating concentrations, CbCh does not induce a complete emptying of microsacs. Channel

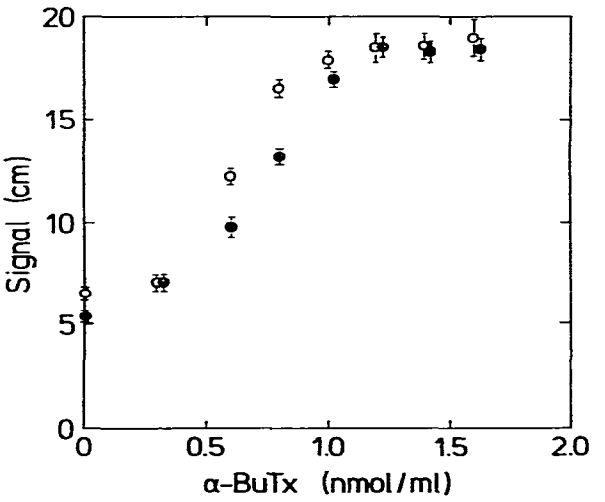

Fig. 3. Reduction of flux amplitudes, expressed as the measured FES signal, with degree of inhibition by α-BuTx, expressed as [α-BuTx] in the incubation bath. The two sets of runs correspond to measurements where, upon exposure to α-BuTx at the indicated concentration, microsacs were (a) injected into flux medium, filtered and the filters washed using the wash sequence leading to a complete emptying of all microsacs containing residual uninhibited receptors (●), (b) injected into 0.5 mM CbCh, filtered and the filters washed with flux medium (○).

closing due to receptor inactivation prevents full equilibration of microsac internal Li^+ with the bath.

The time course of the reduction in flux amplitude due to α-BuTx inhibition was investigated as follows. 5 ml of microsac suspension were injected into 65 ml of an ice-cold α-BuTx solution (0.115 nmol/ml) under stirring. At fixed time intervals after the initial dilution, 5-ml aliquots were removed and injected into a second dilution bath containing 30 ml of ice-cold flux medium. Six filtrations of 5-ml aliquots of the twice-diluted suspension were then performed, each followed by four washings using wash sequence 3 of table I. Fig. 4 presents a plot of the Li^+ content of the filters as a function of the time at which the second dilution was made. Independently, a titration with α-BuTx of the type shown in fig. 3 was carried out using the same suspension. It was verified that the amount of toxin present in the initial dilution bath was slightly in excess of that required to completely abolish flux.

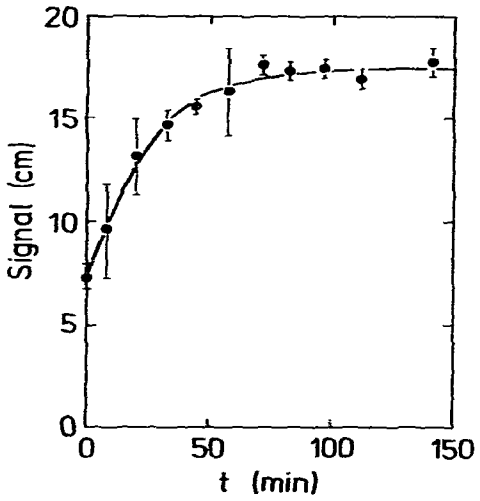

Fig. 4. Time course of the reduction of flux amplitude with progressive inhibition by α-BuTx. Microsacs were injected into a bath containing α-BuTx at time $t=0$. At subsequent times t, aliquots of this mixture were injected into flux medium, filtered and the filters washed using a wash sequence leading to a complete emptying of all microsacs containing residual uninhibited receptors. The curve represents a least-squares simulation using eqs. 2 and 3 of the text, with $\alpha(t)=1-exp(k_{in}t)$, where k_{in} is the apparent rate constant for toxin inhibition. Using the values P_n in table 2, an optimum fit was found for $k_{in}=0.05\ min^{-1}$.

3.4. Filtration using filters with different pore sizes

In order to determine the amount of Li^+ retained on membrane filters of uniform pore sizes 0.45, 0.65, 0.8 and 1.2 μm, aliquots of 0.4 ml of microsac suspension were injected into a dilution bath containing 35 ml of ice-cold flux medium under stirring. Six 5-ml aliquots of the diluted suspension were then filtered, using filters of a given pore size, and washed. For each type of filter, one run using wash sequence 1, and one run using wash sequence 3 of table 1, were carried out. In the former case there should be no flux, in the latter there should be complete emptying of microsacs containing functional receptors. The difference in the Li^+ content of the filters for the two types of runs, shown in fig. 5, represents the Li^+ content of specifically those microsacs retained on the filter that contain functional receptors. Assuming the microsacs are spherical, the cutoff internal volume v_c, corresponding to a filter pore diameter

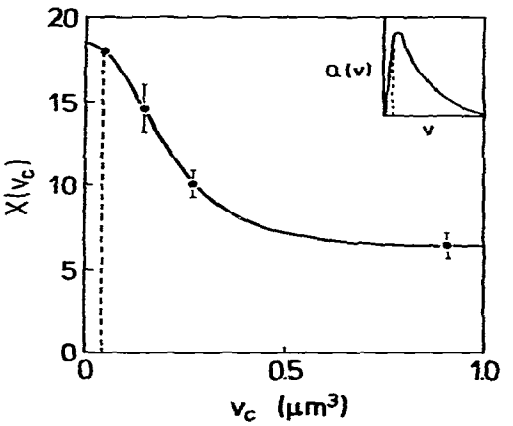

Fig. 5. Li^+ content of filters with cutoff volume v_c expressed as measured FES signal $X(v_c)$. The curve represents a simulation using eq. 4 with the volume distribution function $Q(v)$ given by eq. 5 (see text). The inset represents the optimum $Q(v)$. In the evaluation of v_c for a given pore diameter, the microsac membrane thickness t_m was taken to be 0.01 μm (see text).

d and a microsac membrane thickness t_m, is given by $v_c = (4\pi/3) \cdot [(d/2) - t_m]^3$. Ideally, all microsacs with an internal volume larger than v_c should be retained on the filter. Fig. 5 indicates that with increasing v_c the Li^+ content appears to approach a limiting value. This presumably reflects nonspecific absorption to the filter of microsacs with an internal volume smaller than v_c. Such absorption was previously reported in a study in which a similar filtration technique was utilized to prepare a homogeneous suspension of liposomes [12].

In order to investigate variations in the degree of absorption, the amount of undiluted microsac suspension injected into the 35-ml dilution bath was varied. For filtration using filters of pore size 0.45 μm, the fraction of the total amount of Li^+ added to the filters that was retained remained constant for dilutions up to 1/60, and then increased sharply. The steep increase presumably reflects a progressive clogging of pores leading to retention of microsacs with volumes less than v_c.

4. Analysis of data

4.1. Correction for leakage flux

The sample flux curves shown in fig. 1 indicate that there is no significant leakage efflux of Li^+ on the second to minute time scale. A slow reduction of overall Li^+ content $X(t)$ at time t was detected over a period of hours. Since it took several hours to carry out all steps comprising an experiment (e.g., incubation with toxin), a leakage flux correction was made using the expression

$$X(t) = X(0)e^{-k_l t} \qquad (1)$$

where $X(0)$ is the corrected overall Li^+ content prior to a flux run carried out at time t, and k_l is the rate constant for leakage flux. In order to determine k_l for a given experiment, $X(t)$ was measured at the beginning and end of the experiment. The values of k_l found for several experiments using eq. 1 fell within the range $2(\pm 1) \times 10^{-4}$ min^{-1}. All further analysis of the data will be based implicitly on leakage-corrected values.

4.2. Determination of the fractional internal volume P_n

The reduction of Li^+ content of microsacs preincubated with α-BuTx, as a function of the amount of toxin used, is shown in fig. 3. Independent of the conditions under which flux is measured, there is a progressive increase in Li^+ content with increasing amounts of toxin, until a limiting value is reached. This limiting amount of toxin represents the amount that is required to inhibit all functional receptors. However, it will not necessarily be equal to the number of toxin sites on functional receptors, since part of the toxin may bind to nonfunctional receptors that were damaged in the course of the preparation. A useful measure for expressing the extent of inhibition is the fraction α given by $\alpha =$ (amount of toxin used for incubation/limiting amount) (see fig. 3). For amounts of toxin less than the limiting amount, α represents the fraction of toxin sites on functional receptors that have been inhibited — even if an unknown portion of the total receptors is nonfunctional.

The Li^+ content for flux carried out under conditions leading to complete emptying (fig. 3, filled circles) is due to two contributions: (a) microsacs having no functional receptors will lead to the constant background contribution $X(\alpha = 0)$, measured in the absence of toxin; (b) microsacs having all functional receptors inhibited by toxin will constitute a contribution $X(\alpha) - X(\alpha = 0)$, that increases with α until the limiting value $X(\alpha = 1) - X(\alpha = 0)$ is reached.

It is useful to introduce the relative amplitude change $R(\alpha)$ of the functional microsacs, given by

$$R(\alpha) = [X(\alpha) - X(\alpha = 0)]/[X(\alpha = 1) - X(\alpha = 0)]. \qquad (2)$$

$R(\alpha)$ represents the fractional Li^+ content of functional microsacs having all functional receptors inhibited by toxin. Analysis of the dependences of $R(\alpha)$ on α permits determination of the fractional internal volume P_n of the subfraction of microsacs with n functional receptors per microsac.

In general, a receptor gating unit may contain l independent and equivalent toxin sites, where occupation of a single site suffices to inhibit flux through all channels controlled by the receptor. As

Table 2

Parameters P_n for $l=1$ and $l=2$ (see text)

C_s, concentration of α-BuTx (nmol/ml) at which total inhibition of flux sets in; ϵ, sum of squares of deviations of simulated from measured data.

l	P_1	P_2	P_3	P_4	P_5	P_6	P_7	P_8	C_s	ϵ
1	0.24	0.55	0.20	0.01	0.00	–	–	–	1.06	0.000420
2	0.22	0.08	0.07	0.00	0.06	0.16	0.41	0.00	1.20	0.000072

shown in part II of this series [7] one then obtains

$$R(\alpha)=\sum_{n=1}^{\infty} P_n[1-(1-\alpha)1]^n \qquad (3)$$

where the summation is over the number of functional receptors per microsac. Eq. 3 implies that the flux data expressed in the form of the relationship, eq. 2, can be analysed as a superposition of terms $[1-(1-\alpha)^1]^n$ with unknown coefficients P_n, where $\Sigma_{n=1}^{\infty} P_n = 1$ and $0 \leq P_n \leq 1$. Numerical curve fitting based on a least-squares criterion can be used to determine the P_n. The results of a computer analysis of the toxin inhibition data for

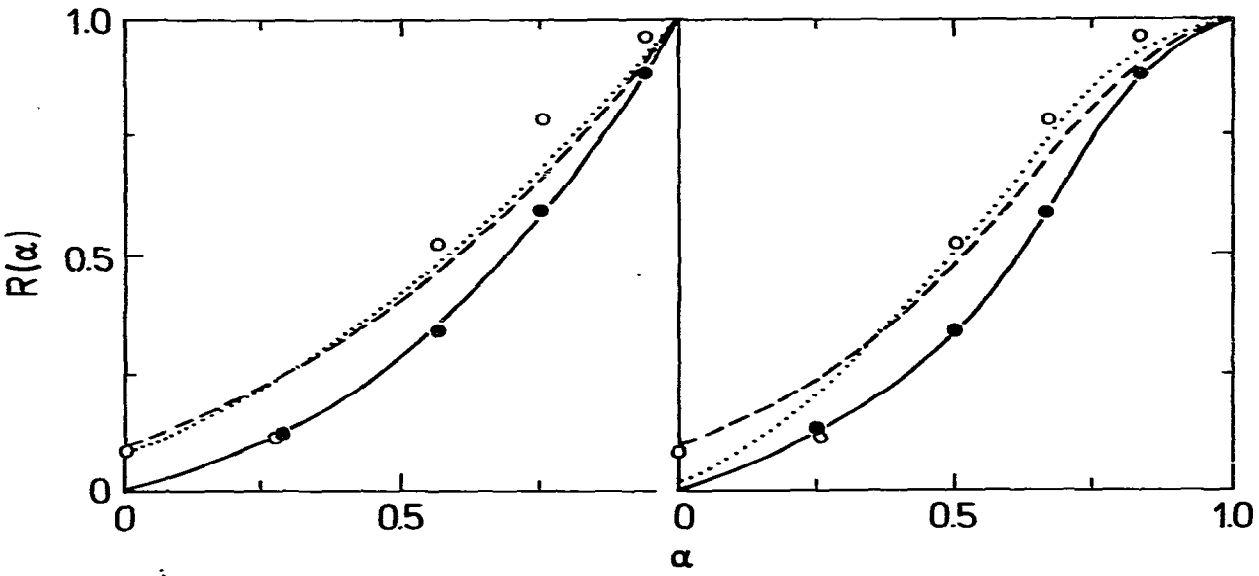

Fig. 6. (Left). Simulation of the dependence of the relative flux amplitude on the fraction of inhibited receptors α assuming a single toxin site per receptor ($l=1$). The data shown in fig. 3 were simulated using eq. 3 to describe flux amplitudes resulting for flux measured under conditions leading to a complete emptying (———), and eqs. 13 and 14, respectively, to describe flux induced by 0.5 mM CbCh for limiting cases I (— — —) and II (· · · · · ·).

Fig. 7. (Right). Simulation of the dependence of the relative flux amplitude on the fraction of inhibited receptors α assuming two toxin sites per receptor ($l=2$). See legend to fig. 6. For flux induced by 0.5 mM CbCh, near identical curves were obtained for simulations based on the assumption that the number of channels r associated with a receptor is one or two.

efflux under conditions leading to a complete emptying of uninhibited microsacs (fig. 3, filled circles) are presented in table 2. As shown in figs. 6 and 7 (solid line), a good fit to the experimental values for $R(\alpha)$ is possible for the cases $l=1$ and $l=2$.

4.3. Determination of the volume distribution function $Q(v)$

A mathematical scheme for analysing the variation in Li^+ content found in flux studies using filters of different pore sizes is presented in the appendix. The data shown in fig. 5 indicate that the Li^+ content $X(v_c)$ decreases with an increase in the cutoff volume v_c corresponding to the pore size of the filter. This measured Li^+ content represents: (a) Li^+ in all functional microsacs with volume larger than v_c, and (b) Li^+ content in all absorbed functional microsacs with volume less than v_c. Assuming that the fraction of microsacs of a given size that is absorbed is a constant independent of microsac size, $X(v_c)$ is given by the empirical relationship eq. A9.

In order to determine $Q(v)$ using eq. A9 it is necessary to adopt one of the trial functions suggested in the appendix. The integral involving $Q(v)$ can then be evaluated explicitly, and curve fitting based on a least-squares criterion may be used to optimize the adjustable parameters. The best possible trial function must be selected on a trial and error basis. The curve in fig. 5 represents a least-squares fit of the equation

$$X(v_c)=A+B\left[\frac{e}{a}^{-av_c}\left(a^2v_c^2+2av_c+2\right)\right] \tag{4}$$

to the measured Li^+ content $X(v_c)$, for a given v_c. This expression results from eq. A9 upon substitution of the normalized trial function (shown in the inset of fig. 5)

$$Q(v)=a^2ve^{-av} \tag{5}$$

where A, B and a are adjustable parameters. The optimum fit was found for $A=6.64$, $B=80.32$ μm^{-3} and $a=13.7$ μm^{-3}. Substitution of eq. 5 into eq. A8 yields the mean volume $\bar{v}$ of the microsacs added to the filter

$$\bar{v}=\frac{2}{a}=0.146\ \mu m^3 \tag{6}$$

Inserting this result together with the values of A and B given above into eq. A10 then yields the fraction of absorbed microsacs $\eta=0.362$. Substitution of eqs. 5 and 6 into eqs. A13 and A7, respectively, yields the fraction $g(v_c)$, of functional microsacs with volume larger than v_c, given by

$$g(v_c)=e^{-av_c}(1+av_c) \tag{7}$$

and the fractional Li^+ content $f(v_c)$, of these microsacs, given by

$$f(v_c)=\frac{e}{2}^{-av_c}\left(a^2v_c^2+2av_c+2\right) \tag{8}$$

The flux amplitude measurements were made using filters of pore diameter $d=0.45$ μm. It is therefore necessary to determine the normalized volume distribution function $Q_{0.45}(v)$, and the mean volume $\bar{v}_{0.45}$, of the microsacs entrapped on such a filter. These quantities will not be identical to the corresponding parameters $Q(v)$ and $\bar{v}$ for the microsac suspension prior to filtration. Inserting the value $\bar{v}_c=0.0477$ μm^3 resulting for pore diameter $d=0.45$ μm into eqs. 7 and 8 yields $g(v_c)=0.860$ and $f(v_c)=0.971$. Substitution of these parameters, together with η determined above, into eqs. A11 and A14 yields

$$Q_{0.45}(v)=\begin{cases}(0.398)Q(v) & v\leq 0.0477\ \mu m^3\\ (0.602)Q(v) & v>0.0477\ \mu m^3\end{cases} \tag{9}$$

and $\bar{v}_{0.45}=(1.078)\bar{v}=0.157$ μm^3.

4.4. Characteristic parameters of the microsacs

As shown previously [7], knowledge of the quantities P_n and $Q(v)$ for a given microsac suspension permits determination of several characteristic parameters. Two limiting cases need to be considered. At low surface densities of receptors there may be little covariance between microsac size and receptor content (case I). At high surface densities the receptor content of a microsac is expected to be proportional to the microsac surface area (case II). using equations previously derived for these cases [7], it is then possible to determine: (a) the fraction of microsacs having n receptors per microsac ξ_n, (b) the mean number of receptors per microsac $\bar{n}$, (c) the mean internal volume $\bar{v}$ and surface area $\bar{s}$ of a microsac, and (d)

Table 3

Fractional receptor content ξ_n

l, number of toxin sites per receptor.

l	Case	ξ_1	ξ_2	ξ_3	ξ_4	ξ_5	ξ_6	ξ_7
1	I	0.24	0.55	0.20	0.01	–	–	–
	II	0.57	0.46	0.09	0.00	–	–	–
2	I	0.22	0.08	0.07	0.00	0.06	0.16	0.41
	II	1.22	0.16	0.07	0.00	0.03	0.06	0.12

the mean surface density of receptors $\bar{\rho}$.

From eq. A8 it follows that $\bar{v}$ can be determined if $Q(v)$ is known. For spherical microsacs, insertion of the value $\bar{v} = 0.146\ \mu m^3$ derived above, into the surface-to-volume relationship $\bar{s} = 4\pi(3\bar{v}/4\pi)^{2/3}$, yields $\bar{s} = 1.34\ \mu m^2$. The remaining parameters given in tables 3 and 4, can be obtained using the values P_n presented in table 2.

4.5. Flux amplitude analysis

The flux amplitudes resulting for Li^+ efflux induced by 0.5 mM CbCh from microsacs preincubated with α-BuTx are presented in fig. 3 (open circles). Unlike in the parallel case (fig. 3, filled circles), where conditions leading to complete emptying of microsacs were used, the CbCh-induced amplitudes will depend not only on the extent of toxin inhibition, but also on channel closing due to receptor inactivation. Using the values $X(\alpha = 0)$ and $X(\alpha = 1)$ for measurements leading to a complete emptying, and $X(\alpha)$ for the CbCh-induced amplitudes, the flux data can again be expressed in terms of the overall relative amplitude change $R(\alpha)$ given by eq. 2. As shown in part II of this series [7], $R(\alpha)$ is given by the general expression

$$R(\alpha) = \sum_{n=1}^{\infty} P_n \left[\langle e^{-kt} \rangle_{\infty}^{n} \right]_v \tag{10}$$

where the square brackets denote averaging over a distribution in microsac internal volume v, and where the mean flux amplitude contribution $\langle e^{-kt} \rangle_{\infty}$ per receptor is given by

$$\langle e^{-kt} \rangle_{\infty} = 1 - (1-\alpha)^{l} \cdot (1 - \langle e^{-kt} \rangle_{u,\infty}^{r}) \tag{11}$$

where l is the number of toxin sites of a receptor, r the number of channels inhibited by occupation of a toxin site, and $\langle e^{-kt} \rangle_{u,\infty}$ the mean single channel flux amplitude contribution. For AcChR-controlled flux at high activator ligand concentrations, one obtains [7] the limiting ligand concentration-independent expression

$$\langle e^{-kt} \rangle_{u,\infty} = \frac{v}{v + (k'_{\mathrm{eff}}/k_i)} \tag{12}$$

where k'_{eff} is the effective volume-independent rate constant for the Li^+-Na^+ exchange flux through a single channel, and k_i the effective forward rate constant for the final slow inactivation phase of the receptor gating reaction. Since v in eq. 12 is a variable, $\langle e^{-kt} \rangle_{u,\infty}$ is uniquely characterized if (k'_{eff}/k_i) is known.

The volume averaging in eq. 10 can be explicitly carried out for the two limiting cases discussed in the preceding section [7]. For case I (limit of low

Table 4

Mean receptor content and mean receptor surface density

l, number of toxin sites per receptor

l	Case	$\bar{n}$	$\bar{\rho}(\mu m^{-2})$
1	I	1.98	1.48
	II	1.78	1.33
2	I	4.72	3.52
	II	3.14	2.34

receptor surface densities) one obtains

$$R(\alpha)=\sum_{n=1}^{\infty} P_n \int_0^{\infty} \langle e^{-kt}\rangle_{\infty} Q_{0.45}(v)\,dv \qquad (13)$$

where $Q_{0.45}(v)$ is given by eq. 9, and $\langle e^{-kt}\rangle_{\infty}$ by eq. 11 with eq. 12. The use of $Q_{0.45}(v)$ rather than $Q(v)$ is indicated, since the measured Li^+ content reflects Li^+ on filters with pore diameter $d=0.45$ μm. Treating the rate constant ratio (k'_{eff}/k_i) in eq. 12 as a variable parameter to be optimized, it is possible to evaluate explicitly eq. 13 by numerical integration. Employing a computer program based on a twelve-point Gaussian integration procedure [13], an optimum fit to the data of fig. 3 (open circles), expressed in terms of eq. 2, was obtained using a least-squares criterion. The results are given in table 5. The best simulation is shown in figs. 6 and 7 (dashed line).

When case II (limit of high receptor surface densities) applies, eq. 10 can be expressed as [7]:

$$R(\alpha)=\sum_{n=1}^{\infty} P_n\left\{1-(1-\alpha)^l\cdot\left[1-\left(\frac{n^{3/2}}{n^{3/2}+c}\right)\right]\right\}^n \qquad (14)$$

where $c=(3/4\pi)\cdot(4\pi\bar{\rho})^{3/2}\cdot(k'_{eff}/k_i)$. Using the value of $\bar{\rho}$ given in table 4, and treating c as a variable to be optimized, least-squares numerical curve fitting of eq. 14 to the data of fig. 3 (open circles), expressed in terms of eq. 2, then leads to the results presented in table 5. The optimum simulation of the data is shown in figs. 6 and 7 (dotted curve).

Table 5

Rate constant ratio for the limiting cases (see text and table 2)

l	r	Case I		Case II	
		(k'/k_d)	ϵ	(k'/k_d)	ϵ
1	1	0.51	0.034	0.51	0.029
2	1	0.26	0.024	0.41	0.014
	2	0.10	0.025	0.18	0.014

5. Discussion

Exposure of *Torpedo marmorata* microsacs containing Li^+ to neuroactivator ligands (e.g., AcCh and CbCh) leads to a reduction of Li^+ content due to efflux of Li^+ through AcChR-controlled transmembrane channels. Under the experimental conditions used in the measurements presented above, flux involves an exchange of microsac internal Li^+ (initial concentration 0.2 M) for Na^+ in the dilution bath (initial concentration 0.2 M). Finite flux amplitudes, reflecting an incomplete emptying of the net microsac Li^+ content, result upon inhibition of receptors by snake toxins, and upon activator ligand-induced receptor inactivation. A detailed mathematical analysis of the activator and/or inhibitor ligand concentration-dependent flux amplitudes was presented in part II of this series [7]. In contrast to previous attempts to analyse the dependence of flux properties on the extent of inhibition by snake toxins [10,14,15], the treatment explicitly accounts for the mixed population of fractionally inhibited microsacs arising upon random binding of toxin to sites localized on the microsacs [4,5]. The resulting general expression for the overall relative flux amplitude $R(\alpha)$ as a function of α, the fraction of total toxin sites occupied, is given by eq. 10 with eq. 11.

Using a novel procedure outlined above, flux can be carried out under conditions leading to a complete emptying of all microsacs containing residual receptors uninhibited by toxin. The α dependence of the resulting flux amplitudes is given by eq. 3. This special case of eq. 10 implies that $R(\alpha)$ is a weighted sum of polynomials in α. Curve fitting can be used to determine the weight factors P_n, and in principle, the number of toxin sites l per receptor gating unit (controlling at least one channel).

When activator ligand-induced flux is carried out under conditions leading to inactivation of receptors, the general expression, eq. 10, for $R(\alpha)$ holds. The mean single channel flux amplitude contribution $\langle e^{-kt}\rangle_{\infty}$ that must then be considered represents the mean factor by which the Li^+ content of a single microsac was reduced due to flux through r channels controlled by a single receptor gating unit. Assuming prior knowledge of

the P_n and l, curve fitting can be used to determine the rate constant ratio (k'_{eff}/k_i), and in principle, r.

Recent investigations of the AcChR of fish electric organs indicate that solubilized receptors exist as monomeric units of subunit structure $\alpha_2\beta\gamma\delta$ ('light form'), or as disulfide-linked dimers of such monomers ('heavy form') [16–18] (see also ref. 19). A given α_2-subunit complex contains one or two activator ligand-binding sites. A Hill coefficient greater than unity has been reported for ligand binding to these sites. A single ion channel is probably associated with each monomeric unit. The binding site for snake toxins is also thought to be on the α-subunits. There is some indication that toxin is bound to two nonequivalent sites (see, e.g., ref. 16).

The measured P_n values for one ($l=1$) or two ($l=2$) equivalent and independent toxin sites per receptor are presented in table 2. Comparison of ϵ, the sum of the squares of the deviations of simulated from measured points, indicates that a slightly better fit is obtained for the case $l=2$. However, the difference is within the limits of confidence of the data points. The various types of fractionally inhibited receptor forms and the corresponding states of the associated ion channels for the cases $l=1$, 2 and $r=1$, 2 have been schematically illustrated in fig. 1 of part II of this series [7]. The case $l=1$ pertains to either (a) a monomeric receptor unit with a single site, or (b) a dimer of mutually independent monomers, with one toxin site per monomer, where occupancy of the site of one monomer would not affect flux controlled by the other monomer. The case $l=2$ pertains either to (a) a monomeric or a dimeric unit, with a total of two sites, where single and double occupancy equally lead to a full inhibition of flux controlled by the respective unit, or (b) to a dimer of mutually independent monomers, with two toxin sites per monomer, where single or double occupancy of a monomer does not affect flux controlled by the other monomer, but does lead to full inhibition of the monomer on which the occupied sites are.

Values for the probability ξ_n, that a given microsac contains n receptors, are given in table 3. For $l=1$ a uniformly varying distribution of ξ_n values is found for limiting cases I and II. For $l=2$ an asymmetric distribution results. The relatively large contribution of ξ_1 for both $l=1$ and $l=2$ excludes the possibility that the receptor is a dimer of mutually independently monomers.

The dose-response curve shown in fig. 2 indicates that flux amplitudes for CbCh-induced Li^+ efflux increase with CbCh concentration until a saturating concentration of approx. 20 μM is reached. At larger concentrations the amplitudes no longer vary significantly. The sample flux data shown in fig. 1 indicate that even at a concentration of 0.5 mM CbCh does not induce a complete emptying of Li^+ content. As shown in figs. 6 and 7, simulation of the flux data by eqs. 13 and 14 correctly reproduces (a) the finite tracer content found for CbCh-induced flux when $\alpha=0$, and (b) the fact that for all values of α, the tracer for CbCh-induced flux is greater than or equal to that for flux under conditions leading to a complete emptying. The fit to the CbCh-induced flux data for $l=2$ is somewhat better than that for $l=1$. However, there is little difference in the simulated curves resulting for subcases $r=1$ and $r=2$.

Cumulatively, the results of the toxin inhibition measurements indicate that the receptor may be a monomeric unit with two toxin sites and one associated channel, or a dimer of two monomers, where each such monomer contains a single toxin site, and where there are either one or two channels associated with the dimer.

The mean receptor surface densities $\bar{\rho}$ given in table 4 are much lower than those estimated to be present in subsynaptic regions [16]. This suggests that both limiting case I (no covariance of microsac size and receptor content) and case II (receptor content is proportional to surface area) need to be considered. The fact that for case II the equality $\Sigma_n \xi_n = 1$ (i.e., normalization condition) is not obeyed for the ξ_n values in table 3 indicates that for both $l=1$ and $l=2$, case II does not strictly hold. Further, the simulated curve corresponding to case I in fig. 6 (dashed curve) shows progressive deviation from the measured points with increasing α. Since an opposite trend is observed for the curve corresponding to case II (dotted curve), the actual degree of correlation between microsac size and receptor content lies between that for case I and case II.

The optimum (k'_{eff}/k_i) values obtained from curve fitting are given in table 5. In spite of some variations for cases I and II, and for $l=1$ and $l=2$, the values fall in the relatively narrow range $0.10 \leq k'_{eff}/k_i \leq 0.51$. k'_{eff} is the effective rate constant for flux through a single channel on a microsac with unit volume 1 μm^3. The effective rate constant k_{eff}, for flux through a single channel on a microsac with internal volume v, is given by $k_{eff} = k'_{eff}/v$. Substituting the mean volume $\bar{v} = 0.147$ μm^3, one obtains the mean range of values of $0.68 \leq k_{eff}/k_i \leq 3.47$. Mean flux through a single channel thus occurs on the same time scale as slow receptor inactivation (i.e., the time scale of seconds [16]). As shown previously [7], k_{eff} is given by the product $k_{eff} = k \cdot \Pi_j \alpha^{(o)}_{j,eq}$, where $\alpha^{(o)}_{j,eq}$ represents the equilibrium fraction of open channels following completion of the jth phase of the receptor gating reaction, and k is the (true) rate constant for tracer flux through a permanently open channel. If $\alpha^{(o)}_{j,eq} < 1$ for any phase j preceding the slowest inactivation mode, then $k_{eff} < k$. Recent evidence suggests that the activator ligand-induced AcChR gating reaction involves at least three phases on separate time scales [16]. In part II of this series [7] it was suggested that in the limit of high activator ligand concentrations, a linear reaction pathway involving a rapid activation step followed by intermediate and slow inactivation steps is expected to constitute a reaction scheme of minimum complexity for the AcChR gating reaction. It was shown that for such a linear scheme the quality $k'_{eff}/k_i = k/k_d$ holds, where k_d is the forward rate constant for the slow inactivation step. The above findings would therefore indicate that the true (activator concentration independent) rate constant k_d is of the order of k, while the effective mode rate coefficient k_i is of the order of k'_{eff}.

The unusually low $\bar{p}$ values in table 4 may arise because (a) the microsacs used were from a low-density fraction of the Percoll gradient [8], and (b) a portion of the receptors may have been damaged during the preparation, and thus rendered nonfunctional. An incorrect value of $\bar{p}$ could result if irreversible binding of toxin to receptor sites were more rapid then mixing of the diluted microsacs in the incubation step. Local inhomogeneities in toxin concentration might then arise, leading to nonrandom binding. However, the data presented in fig. 4 show that inhibition occurs on the time scale of minutes, and is thus much slower than mixing. An incorrect value of $\bar{p}$ would also be obtained if the toxin sites were not equivalent and independent. Positive cooperativity in toxin binding would lead to an underestimation, and negative cooperativity to an overestimation, of $\bar{p}$. Although the possibility of cooperativity cannot be excluded, positive cooperativity due primarily to charge effects seems implausible. The receptor has a net negative charge while α-BuTx has a net positive charge. Therefore toxin binding would lead to increasing neutralization of charge, reducing the probability of capture of toxin molecules on the microsac surface.

As has been shown elsewhere [5], the method of progressive toxin inhibition of flux employed above to determine the parameters P_n can only be used if $\bar{p}$ is small, so that for a predominant portion of the microsacs $n \lesssim 50$. A more generally applicable approach valid for arbitrary $\bar{p}$ is being developed (J. Bernhardt and E. Neumann, to be published).

In summary, experimental techniques for determining fundamental parameters required for a quantitative analysis of gated tracer flux from or into microsacs have been presented. The quantities P_n and $Q(v)$ reflect the distribution in microsac size and receptor content, which may vary from preparation to preparation. They are intrinsic parameters of a given collection of microsacs, and do not depend on the nature and concentration of the tracer species used. Thus, although efflux of Li^+ was used as a mode of measurement in the present work, the values of P_n and $Q(v)$ determined above could be used in the analysis of all subsequent measurements with the same microsacs — even if another tracer species and another mode of measurement were employed. Knowledge of the parameters permits determination of the mean single channel flux contribution $\langle e^{-kt} \rangle$. In analogy with the investigation of flux amplitudes reported above, the following general steps can be employed to analyse flux data: (1) Characterization of parameters P_n and $Q(v)$ for a given microsac suspension; (2) Substitution of k'/v for k in the expression for $\langle e^{-kt} \rangle$ appropriate to the gating

process being investigated; (3) Explicit evaluation of the volume averages in eqs. A6 and A7 for the two limiting cases of no covariance, and of strong covariance, of the distributions in receptor content and size; (4) Determination of the volume-independent terms in $\langle e^{-kt} \rangle$; (5) Further analysis of these terms based on examination of their dependence on the concentration of control ligands.

Acknowledgements

We would like to thank Dr. K.M. Moss and R.M. Luckinger for their assistance in the preparation of the microsacs. We greatefully acknowledge financial support by the Deutsche Forschungsgemeinschaft, Grant NE 227.

Appendix

The tracer content $X(v_c)$ of a filter with cutoff internal volume v_c is given by

$$X(v_c) = X(0)\{f(v_c) + [1 - f(v_c)]\eta(v_c)\} \tag{A1}$$

where $X(0)$ is the total amount of tracer in the microsacs added to the filter, $f(v_c)$ the fraction of $X(0)$ in microsacs with volume larger than v_c, and $\eta(v_c)$ the fraction of the microsacs with volume less than v_c that are absorbed to the filter. $f(v_c)$ is a uniformly decreasing function of v_c, where $f(0) = 1$ and $\lim_{v_c \to \infty} f(v_c) = 0$. The dependence of $\eta(v_c)$ on v_c is expected to be determined by many factors, e.g., the surface area of the filters, the presence of cavities suitable for accommodating microsacs of a given size, and the degree of saturation of the available absorption sites. In filtration experiments using *Torpedo* microsacs, it was commonly found that the measured $X(v_c)$ reaches a limiting value $X(\infty)$ with increasing v_c, given by

$$X(\infty) = \lim_{v_c \to \infty} X(v_c) = X(0) \lim_{v_c \to \infty} \eta(v_c) = X(0)\eta(\infty) \tag{A2}$$

where $\eta(\infty)$ is the limiting value of $\eta(v_c)$ for filters with large pore size.

Considerable simplification results if the fraction of microsacs of a given volume v, that are absorbed, has the constant, volume-independent value η. From eq. A2 one obtains

$$\eta = \eta(\infty) = X(\infty)/X(0). \tag{A3}$$

Substitution of η given by eq. A3 for $\eta(v_c)$ in eq. A1 then yields

$$X(v_c) = X(\infty) + [X(0) - X(\infty)] \cdot f(v_c). \tag{A4}$$

The amount of tracer in all microsacs with internal volume v is given by $\nu \cdot C_o \cdot v \cdot Q(v)$, where ν is the total number of microsacs, C_o the concentration of tracer in each microsac, and $Q(v)$ the probability that a given microsac has the internal volume v. The total tracer content $Y(v_c)$, of the microsacs with internal volume larger than v_c is therefore given by

$$Y(v_c) = \nu C_o \int_{v_c}^{\infty} vQ(v)\,dv \tag{A5}$$

where $Q(v)$ obeys the normalization condition

$$\int_0^{\infty} Q(v)\,dv = 1 \tag{A6}$$

The fractional tracer content $f(v_c)$ in the microsacs with volume larger than v_c is given by

$$f(v_c) = Y(v_c)/Y(0) = \frac{1}{\bar{v}} \int_{v_c}^{\infty} vQ(v)\,dv \tag{A7}$$

with the mean internal volume $\bar{v}$ defined by

$$\bar{v} = \int_0^{\infty} vQ(v)\,dv. \tag{A8}$$

Substitution of eq. A7 into eq. A4 yields the empirical relationship expressing the dependence of $X(v_c)$ on v_c

$$X(v_c) = A + B \int_{v_c}^{\infty} vQ(v)\,dv \tag{A9}$$

where A and B are constants. Noting that $A = X(\infty)$ and $B = [X(0) - X(\infty)]/\bar{v}$, one obtains from eq. A3

$$\eta = \frac{A}{A + Bv} \tag{A10}$$

In principle, the functional dependence of $Q(v)$ on v could be of arbitrary complexity. Plausibility

arguments suggest that $Q(v)$ passes through a single maximum, and that $\lim_{v\to 0} Q(v) = \lim_{v\to\infty} Q(v) = 0$. While $Q(v)$ could be determined by numerical differentiation of eq. A9, a less tedious approach is to substitute an approximate trial function for $Q(v)$ in eq. A9. Optimization based on least-squares fitting to the measured $X(v_c)$ values can then be used to determine the constants A and B, as well as variable parameters contained in the trial functions. Candidate trial functions of suitable functional form are the functions $v^n \cdot \exp[-a \cdot v]$ and $v^n \cdot \exp[-a \cdot (v - \bar{v})^2/2\pi\sigma^2]$, where a, $\bar{v}$, σ and n are variable parameters. After appropriate normalization based on eq. A6, these trial functions, or linear combinations thereof, can be used to approximate $Q(v)$ in the range $0 \leq v \leq \infty$.

$Q(v)$ is the normalized volume distribution function for the microsac suspension prior to filtration. In order to describe the volume distribution of microsacs entrapped on a filter with pore diameter d, it is useful to introduce the normalized distribution functions $Q_d(v)$. For $v \leq v_c$, $Q_d(v)$ must reflect the volume distribution of the absorbed microsacs, given by $\eta Q(v)$. For $v > v_c$, $Q_d(v)$ will be given by $Q(v)$. Noting that $Q_d(v)$ must obey the same normalization condition as $Q(v)$, one obtains

$$Q_d(v) = \begin{cases} \phi \cdot Q(v) & v \leq v_c \\ (1-\phi) \cdot Q(v) & v > v_c \end{cases} \tag{A11}$$

where ϕ is given by

$$\phi = \frac{\eta}{\eta + (1-\eta) g(v_c)} \tag{A12}$$

with $g(v_c)$, the fraction of microsacs with internal volume greater than v_c, given by

$$g(v_c) = \int_{v_c}^{\infty} Q(v)\, dv. \tag{A13}$$

Substituting $Q_d(v)$ for $Q(v)$ in eq. A8 yields the mean internal volume $\bar{v}_d$ of the microsacs entrapped on a filter with pore diameter d. One obtains

$$\bar{v}_d = \bar{v} \cdot \left[\frac{\eta + (1-\eta) \cdot f(v_c)}{\eta + (1-\eta) \cdot g(v_c)} \right] \tag{A14}$$

where $\bar{v}$ is the mean internal volume of the microsacs prior to filtration.

References

1 M. Kasai and J.-P. Changeux, J. Membrane Biol. 6 (1981) 1.
2 J. Bernhardt and E. Neumann, Proc. Natl. Acad. Sci. U.S.A. 75 (1978) 3756.
3 J.W. Walker, M.G. McNamee, E. Pasquale, D.J. Cash and G.P. Hess, Biochem. Biophys. Res. Commun. 100 (1981) 86.
4 J. Bernhardt and E. Neumann, J. Theor. Biol. 86 (1980) 649.
5 J. Bernhardt and E. Neumann, Neurochem. Int. 2 (1980) 243.
6 J. Bernhardt and E. Neumann, Biophys. Chem. 14 (1981) 303.
7 J. Bernhardt and E. Neumann, Biophys. Chem. 15 (1982) 317.
8 J. Bernhardt, K.M. Moss, R.M. Luckinger and E. Neumann, FEBS Lett. 134 (1981) 245.
9 D.L. Miller, H.P.H. Moore, P.R. Hartig and M.A. Raftery, Biochem. Biophys. Res. Commun. 85 (1978) 632
10 H.P.H. Moore, P.R. Hartig and M.A. Raftery, Proc. Natl. Acad. Sci. U.S.A. 76 (1980) 6265.
11 R.R. Neubig and J.B. Cohen, Biochemistry 19 (1980) 2770.
12 S.E. Schullery and J.P. Garzaniti, Chem. Phys. Lipids 12 (1973) 75.
13 S.D. Conte, Elementary Numerical Analysis (McGraw-Hill, New York, 1965).
14 S.M. Sine and P. Taylor, J. Biol. Chem. 255 (1980) 10144.
15 S.M. Sine and P. Taylor, J. Biol. Chem. 256 (1981) 6692.
16 J.-P. Changeux, in: Harvey Lectures 75 (1981) 85.
17 M.A. Raftery, M.W. Hunkapiller, C.D. Strader and L.E. Hood, Science 208 (1980) 1454.
18 A. Karlin, in: The Cell Surface and Neuronal Function, eds. C.W. Cotman, G. Poste and G.L. Nicholson (Elsevier/North-Holland Biomedical Press, Amsterdam, 1980), p. 191.
19 E. Neumann and J. Bernhardt, J. Physiol. (Paris) 77 (1981) 30.